Sensors & Transducers, Vol. 226, Issue 10, October 2018, pp. 93-99

www.sensorsportal.com

Sensors & Transducers

Published by IFSA Publishing, S. L., 2018
http://www.sensorsportal.com

Generation of Fixed-position Foci with Generalized Fibonacci Class Zone Plate

[1] Tian Xia, [3] Shubo Cheng and [1, 2, *] Shaohua Tao

[1] School of Physics and Electronics, Central South University, Changsha 410083, China
[2] Hunan Key Laboratory of Super Microstructure and Ultrafast Process, Central South University, Changsha 410083, China
[3] School of Physics and Optoelectronic Engineering, Yangtze University, Jingzhou, Hubei 434023, China
[*] E-mail: eshtao@csu.edu.cn

Received: 25 June 2018 /Accepted: 31 August 2018 /Published: 31 October 2018

Abstract: In this paper the generalized Fibonacci class zone plates with varying structural parameters are proposed to generate the fixed-position foci. Unlike the generalized Fibonacci and modified Thue-Morse zone plates, the proposed zone plate can generate more subsidiary foci and the construction method is applicable to many kinds of bi-focal zone plates. The construction method of the proposed zone plate is illustrated and the focusing property of the proposed zone plate has been verified with simulations. The Fibonacci, Thue-Morse, m-bonacci and precious mean sequences are the common bi-focal sequences. It was proved in the simulation that the position of one of the foci of a generalized Fibonacci class zone plate based on the common bi-focal sequence can be kept constant when the structural parameters change and the generalized Fibonacci class zone plates based on the common bi-focal sequences can generate more subsidiary foci along the optic axis, and the position of one of two main foci can be kept constant for two different generalized Fibonacci class zone plates based on the arbitrary-order common bi-focal sequences. The proposed zone plates can be applied to trap particles at the designated plane and generate a clearer image at the described position along the optic axis.

Keywords: Fibonacci class sequence, Generalized Fibonacci class zone plate, Fixed-position foci, Twin foci, Bi-focal zone plate.

1. Introduction

Fixed-position foci surrounded by the subsidiary foci can be generated by the aperiodic zone plates and have many applications [1]. For example, a fixed-position focus with many subsidiary foci can be used to reduce the chromatic aberration of optical imaging [2], generate multiple vortices [3] and trap particles in the designated planes simultaneously [4-5].

Illustrated with a collimated laser beam, Fibonacci zone plates can generate twin main foci with a position ratio of the golden mean and equal intensity [6]. Similarly, Thue-Morse zone plates produce twin main foci surrounded by many subsidiary foci with equal intensity and can be used to reduce chromatic aberration in optical imaging [7]. Composite Thue-Morse zone plates enhance the intensities of the twin main foci generated by the Thue-Morse zone plates [8]. M-bonacci zone plates can generate twin main foci located at the positions related to a ratio of the m-golden mean [9-10]. The generalized mean zone plate can generate twin foci with the generalized mean, which includes the m-golden mean, precious mean and so on [11]. However, when the structural parameters

of theses zone plates vary, the focal positions will change, too. Although the generalized Fibonacci zone plates with the special seeds produce twin foci with the fixed positions [12] and the modified Thue-Morse zone plates with the optical path difference method and the modified structure can generate twin foci located at the fixed positions [13-14], the zone plates generate few subsidiary foci, which would be unfavorable in the reduction of chromatic aberration. Generally speaking, the above-mentioned zone plates with varying structural parameters are difficult to generate a fixed-position focus with more subsidiary foci.

In recent years, the aperiodic photonic crystals have been found to possess many unique properties. For instance, the fractal photonic crystals can generate self-similarity transmission spectrum [15] and Fibonacci photonic crystals can generate omnidirectional band gaps, mode beating and strong pulse stretching [16-17]. Thus, the photonic crystal based on the proposed sequence will also have many study-worthy properties.

In this paper we will propose a generalized Fibonacci class zone plate (GFiCZP). With varying structural parameters, the GFiCZPs can generate a fixed-position focus and more subsidiary foci along the optic axis. The construction method of the proposed zone plate is general and can be applied to construct many kinds of bi-focal zone plates. The focusing properties of the GFiCZP will be studied with simulations.

2. Design

As we know, a zone plate consists of alternate transparent (A) and opaque (B) zones. The common bi-focal zone plates such as Fibonacci, Thue-Morse, m-bonacci and precious mean zone plates are constructed on the basis of the Fibonacci, Thue-Morse, m-bonacci and precious mean sequences [14], respectively. For the GFiCZP, n Bs are added in front of each letter A of the above-mentioned sequences. n is a non-negative integer and represents the count of the added Bs. The modified sequences are of the generalized Fibonacci class sequences, which include the Fibonacci class sequences based on the substitution rules of $A \rightarrow B^nAB$ and $B \rightarrow B^nA$ related to the precious mean sequences [14]. The Fibonacci, Thue-Morse, m-bonacci and precious mean sequences are the corresponding generalized Fibonacci class sequences with n=0. For simplicity, the Fibonacci sequence of the fifth order is taken for an example to illustrate the construction method of the generalized Fibonacci class sequence. Fig. 1(a) and Fig. 1(b) show the Fibonacci sequence of the fifth order and the corresponding generalized Fibonacci class sequence, respectively.

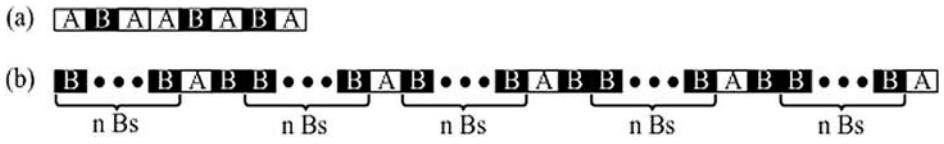

Fig. 1. Schematics of (a) the Fibonacci sequence and (b) the generalized Fibonacci class sequence of the fifth order.

In fact, the Fibonacci sequence of the fifth order in Fig. 1(a) is also the corresponding generalized Fibonacci class sequence with n=0 in Fig. 1(b). It is worth mentioning that the GFiCZP can be generated with a transmission function $q(\zeta)$ based on the generalized Fibonacci class sequence. The transmission function $q(\zeta)$ is written as (1),

$$q(\zeta)=\sum_{j=1}^{N_S} t_{S,j}\cdot rect\left[\frac{\zeta-(j-1/2)\cdot d_S}{d_S}\right], \qquad (1)$$

where $\zeta=(r/a)^2$, $\zeta\in[0,1]$ is the normalized square radial coordinate, S is the order, and N_S is the total count of the elements for the generalized Fibonacci class sequence of the S-th order. In Equation (1), $t_{S,j}$ is "1" or "0" when the j^{th} element of the corresponding generalized Fibonacci class sequence is "A" or "B", respectively. Thus, the sequence of each order consists of N_S equal parts, and each part has the same length of $d_S=1/N_S$. Figs. 2(a-d) show the transmittance pupil functions of the Fibonacci, Thue-Morse, 3-bonacci and silver mean zone plates of the fourth order, respectively. It should be noted that the 3-bonacci sequence is the m-bonacci sequence with m=3 [9] and the silver mean sequence is the special case of the precious mean sequence [14].

Figs. 3(a-d) show the transmittance pupil functions of the corresponding GFiCZPs with n=2, respectively.

3. Focusing Properties of the GFiCZP

When a collimated laser beam passes through a GFiCZP, the axial irradiance of the GFiCZP can be calculated with the Fresnel approximation in (2) [7],

$$I(u)=4\pi u^2\left|\int_0^1 q(\zeta)\exp(-2\pi u\zeta)d\zeta\right|^2 \qquad (2)$$

Combining (1) and (2) one can obtain (3),

$$I(u)=\frac{1}{\pi}\left|i\sum_{j=1}^{N_S}t_{S,j}(e^{-i2\pi ujd_S}-e^{-i2\pi u(j-1)d_S})\right|^2 \quad (3)$$

In Equation (2), $u=a^2/(2\lambda z)$ is the reduced axial coordinate, λ is the wavelength of light and z is the axial distance from the zone plate. From Equation (3) we can obtain intensity of the beam at any axial position.

For convenience, the fifth-order Fibonacci, fourth-order Thue-Morse, fifth-order 3-bonacci and fourth-order silver mean sequences are taken together for comparison to study the focusing properties of the GFiCZPs. Figs. 4(a-d) show the axial intensity distributions of the GFiCZPs based on the Fibonacci, Thue-Morse, 3-bonacci and silver mean sequences, respectively.

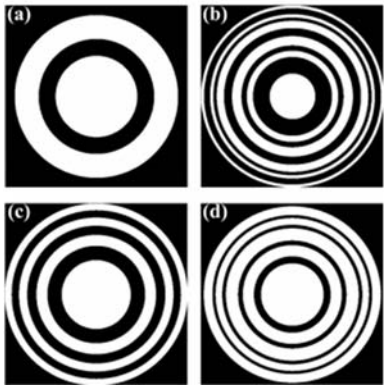

Fig. 2. Transmissions of (a) the Fibonacci, (b) Thue-Morse, (c) 3-bonacci and (d) silver mean zone plates of the fourth order, respectively.

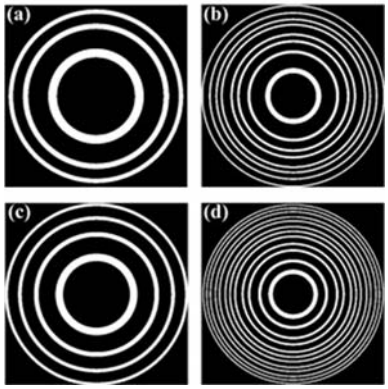

Fig. 3. Transmissions of the GFiCZPs with n=2 based on (a) the Fibonacci, (b) Thue-Morse, (c) 3-bonacci and (d) silver mean sequences of the fourth order, respectively.

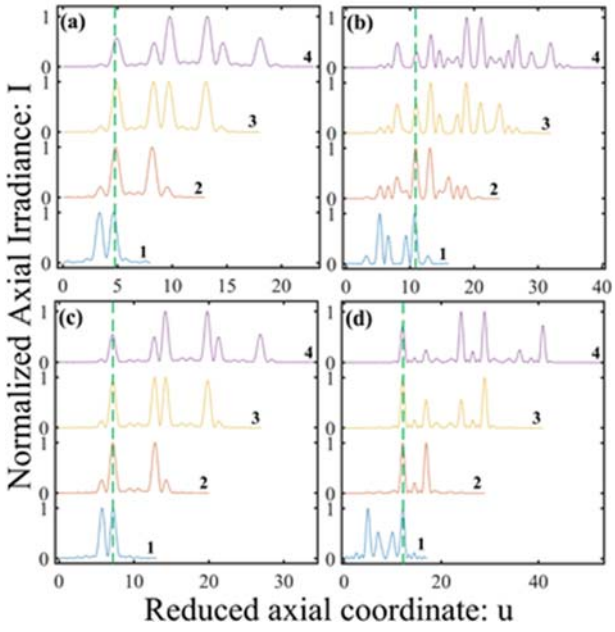

Fig. 4. The axial intensity distributions of the GFiCZPs with n=0, 1, 2 and 3 based on (a) the Fibonacci, (b) Thue-Morse, (c) 3-bonacci and (d) silver mean sequences, respectively.

Lines 1-4 in Fig. 4(a) show the axial intensity distributions of the GFiCZPs based on the Fibonacci sequence with n=0, 1, 2 and 3, respectively. Lines 1-4 in Figs. 4(b-d) show the axial intensity distributions of the GFiCZPs based on the Thue-Morse, the 3-bonacci and the silver mean sequences, where n=0, 1, 2 and 3, respectively. It can be seen from Fig. 4(a) that the *u* values of the foci in lines 1-4 around the dashed lines are [4.64, 4.82, 4.89, 4.94], respectively. The *u* values of the corresponding foci in Figs. 4(b-d) are [10.71, 10.87, 10.96, 11.02], [7.23, 7.19, 7.15, 7.14] and [12.10, 12.09, 12.08, 12.07], respectively. Thus, the *u* values around the dashed lines for the main or subsidiary foci in Figs. 4(a-d) are approximately the

same. Therefore, the position of one of the foci of the GFiCZPs can be kept constant with varying structural parameters. The distributions of the subsidiary foci in lines 3 and 4 are denser than those in lines 2 and 3, respectively. Thus, the GFiCZP can generate more subsidiary foci along the optic axis. Interestingly, it can be seen from Fig. 4(a) that the *u* values of two main foci in lines 1-4 are [(3.36, 4.64), (4.82, 8.18), (4.89, 13.11), (9.78, 13.22)], respectively. The corresponding *u* values of two main foci in Figs. 4(b-d) are [(5.28, 10.72), (10.87, 13.13), (13.21, 18.79), (18.86, 21.14)], [(5.77, 7.23), (7.18, 12.82), (12.76, 14.24), (14.20, 19.80)] and [(4.90, 12.10), (12.09, 16.91), (12.07, 28.93), (24.10, 28.90)], respectively. It can be observed that the *u* values of one of two main foci are approximately the same for lines 1-2, 2-3 and 3-4 in Fig. 4(a). The same property can be found in Figs. 4(b-d). Therefore, the positions of one of two foci can also be kept constant for two different GFiCZPs.

In fact, the GFiCZPs based on the arbitrary-order bi-focal sequences have the same focusing property. In the following, we will study the focusing properties of the GFiCZPs based on the arbitrary-order bi-focal sequences, such as the Fibonacci, Thue-Morse, 3-bonacci and silver mean sequences and so on.

Firstly, Figs. 5(a-c) show the axial intensity distributions of the GFiCZPs based on the Fibonacci sequences of S=4, 5 and 6, respectively. Lines 1-4 in Fig. 5(a) show the axial intensity distributions of the GFiCZPs with n=0, 1, 2 and 3 based on the Fibonacci sequence of S=4. Lines 1-4 in Fig. 5(b) and Fig. 5(c) show the axial intensity distributions of the referred other GFiCZPs, respectively. It can be seen from Fig. 5(a) that the *u* values of the foci in lines 1-4 around the dashed lines are [3.15, 3.19, 3.19, 3.19], respectively. The *u* values of the corresponding foci in Fig. 5(b) and Fig. 5(c) are [4.64, 4.81, 4.89, 4.92] and [8.06, 8.08, 8.08, 8.08], respectively. It can be observed that the *u* values for the foci around the dashed lines in Figs. 5(a-c) are approximately the same. Therefore, the position of one of the foci of a GFiCZP based on the arbitrary-order Fibonacci sequence can be also kept constant when the structural parameters change. The subsidiary foci in lines 3 and 4 are more than those in lines 2 and 3, respectively. Thus, the GFiCZP based on the Fibonacci sequence can generate more subsidiary foci along the optic axis. Interestingly, it can be seen from Fig. 5(a) that the *u* values of two main foci in lines 1-4 are [(1.85, 3.15), (3.19, 4.81), (3.19, 7.81), (6.21, 7.79)], respectively. The corresponding *u* values of two main foci in Fig. 5(b) and Fig. 5(c) are [(3.36, 4.64), (4.81, 8.19), (4.89, 13.11), (9.78, 13.22)] and [(4.94, 8.06), (8.08, 12.92), (8.08, 20.92), (16.10, 20.90)], respectively. Thus, the *u* values of one of two main foci are approximately the same for lines 1-2, 2-3 and 3-4 in Fig. 5(a). The same property applies for the lines in Fig. 5(b) and Fig. 5(c). Therefore, the position of one of two foci can be kept constant for two different GFiCZPs based on the arbitrary-order Fibonacci sequences.

Next, Figs. 6(a-c) show the axial intensity distributions of the GFiCZPs based on the Thue-Morse sequences of S=3, 4 and 5, respectively. Lines 1-4 in Fig. 6(a) show the axial intensity distributions of the GFiCZPs with n=0, 1, 2 and 3 based on the Thue-Morse sequence of S=3. Lines 1-4 in Fig. 6(b) and Fig. 6(c) show the axial intensity distributions of the referred other GFiCZPs, respectively. It can be seen from Fig. 6(a) that the *u* values of the foci in lines 1-4 around the dashed lines are [5.13, 5.24, 5.29, 5.32], respectively. The *u* values of the corresponding foci in Fig. 6(b) and Fig. 6(c) are [10.71, 10.87, 10.96, 11.02] and [21.17, 21.20, 21.21, 21.22], respectively. It can be observed that the *u* values for the foci around the dashed lines in Figs. 6(a-c) are approximately the same. Therefore, the position of one of the foci of a GFiCZP based on the arbitrary-order Thue-Morse sequence can be also kept constant when the structural parameters change. The subsidiary foci in lines 3 and 4 are more than those in lines 2 and 3, respectively. Thus, the GFiCZP based on the Thue-Morse sequence can generate more subsidiary foci along the optic axis. Interestingly, it can be seen from Fig. 6(a) that the *u* values of two main foci in lines 1-4 are [(2.87, 5.13), (5.24, 6.76), (6.81, 9.19), (9.23, 10.77)], respectively. The corresponding *u* values of two main foci in Fig. 6(b) and Fig. 6(c) are [(5.29, 10.71), (10.87, 13.13), (13.21, 18.79), (18.85, 21.15)] and [(10.83, 21.17), (21.20, 26.80), (26.81, 37.19), (37.20, 42.80)], respectively. Thus, the *u* values of one of two main foci are approximately the same for lines 1-2, 2-3 and 3-4 in Fig. 6(a). The same property applies for the lines in Fig. 6(b) and Fig. 6(c). Therefore, the position of one of two foci can be kept constant for two different GFiCZPs based on the arbitrary-order Thue-Morse sequences.

Then, Figs. 7(a-c) show the axial intensity distributions of the GFiCZPs based on the 3-bonacci sequences of S=5, 6 and 7, respectively. Lines 1-4 in Fig. 7(a) show the axial intensity distributions of the GFiCZPs with n=0, 1, 2 and 3 based on the 3-bonacci sequence of S=5. Lines 1-4 in Fig. 7(b) and Fig. 7(c) show the axial intensity distributions of the referred other GFiCZPs, respectively. It can be seen from Fig. 7(a) that the *u* values of the foci in lines 1-4 around the dashed lines are [7.23, 7.19, 7.16, 7.14], respectively. The *u* values of the corresponding foci in Fig. 7(b) and Fig. 7(c) are [13.04, 13.04, 13.04, 13.04] and [23.75, 23.85, 23.89, 23.92], respectively. It can be observed that the *u* values for the foci around the dashed lines in Figs. 7(a-c) are approximately the same. Therefore, the position of one of the foci of a GFiCZP based on the arbitrary-order 3-bonacci sequence can be also kept constant when the structural parameters change. The subsidiary foci in lines 3 and 4 are more than those in lines 2 and 3, respectively. Thus, the GFiCZP based on the 3-bonacci sequence can generate more subsidiary foci along the optic axis. Interestingly, it can be seen from Fig. 7(a) that the *u* values of two main foci in lines 1-4 are [(5.77, 7.23), (7.19, 12.81), (12.76, 14.24), (14.20, 19.80)], respectively. The corresponding *u* values of two main

foci in Fig. 7(b) and Fig. 7(c) are [(10.96, 13.04), (13.04, 23.97), (13.04, 36.93), (26.04, 36.96)] and [(20.25, 23.75), (23.85, 44.15), (23.89, 68.01), (47.82, 68.18)], respectively. Thus, the *u* values of one of two main foci are approximately the same for lines 1-2, 2-3 and 3-4 in Fig. 7(a). The same property applies for the lines in Fig. 7(b) and Fig. 7(c). Therefore, the position of one of two foci can be kept constant for two different GFiCZPs based on the arbitrary-order 3-bonacci sequences.

Finally, Figs. 8(a-c) show the axial intensity distributions of the GFiCZPs based on the silver mean sequences of S=4, 5 and 6, respectively. Lines 1-4 in Fig. 8(a) show the axial intensity distributions of the GFiCZPs with n=0, 1, 2 and 3 based on the silver mean sequence of S=4. Lines 1-4 in Fig. 8(b) and Fig. 8(c) show the axial intensity distributions of the referred other GFiCZPs, respectively. It can be seen from Fig. 8(a) that the *u* values of the foci in lines 1-4 around the dashed lines are [4.54, 4.79, 4.89, 4.92], respectively. The *u* values of the corresponding foci in Fig. 8(b) and Fig. 8(c) are [12.10, 12.09, 12.07, 12.07] and [28.89, 28.96, 28.97, 28.98], respectively. It can be observed that the *u* values for the foci around the dashed lines in Figs. 8(a-c) are approximately the same. Therefore, the position of one of the foci of a GFiCZP based on the arbitrary-order silver mean sequence can be also kept constant when the structural parameters change. The subsidiary foci in lines 3 and 4 are more than those in lines 2 and 3, respectively. Thus, the GFiCZP based on the silver mean sequence can generate more subsidiary foci along the optic axis. Interestingly, it can be seen from Fig. 8(a) that the *u* values of two main foci in lines 1-4 are [(2.46, 4.54), (4.79, 7.21), (4.89, 12.11), (9.77, 12.23)], respectively.

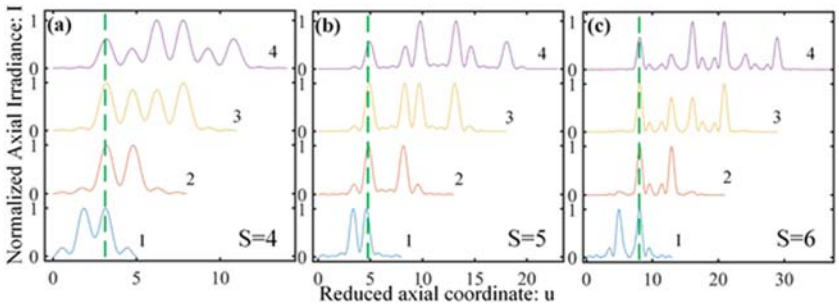

Fig. 5. The axial intensity distributions of the GFiCZPs based on the Fibonacci sequences of S=(a) 4, (b) 5 and (c) 6, respectively. For the GFiCZPs in each sub-figure, n=0, 1, 2 and 3, respectively.

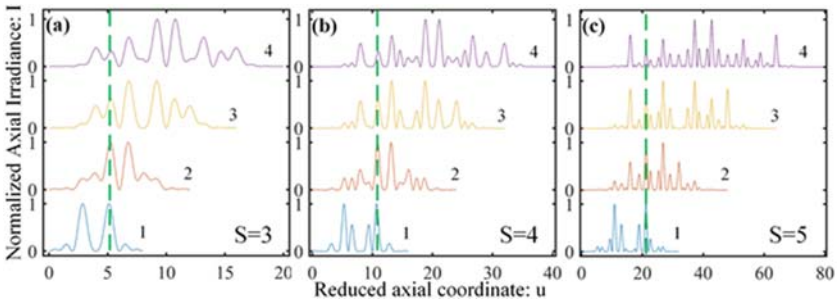

Fig. 6. The axial intensity distributions of the GFiCZPs based on the Thue-Morse sequences of S=(a) 3, (b) 4 and (c) 5, respectively. For the GFiCZPs in each sub-figure, n=0, 1, 2 and 3, respectively.

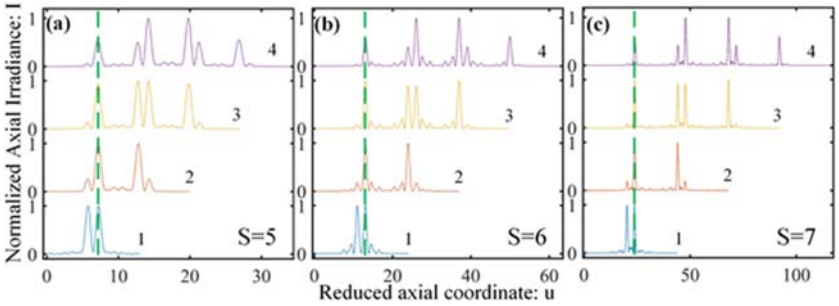

Fig. 7. The axial intensity distributions of the GFiCZPs based on the 3-bonacci sequences of S=(a) 5, (b) 6 and (c) 7, respectively. For the GFiCZPs in each sub-figure, n=0, 1, 2 and 3, respectively.

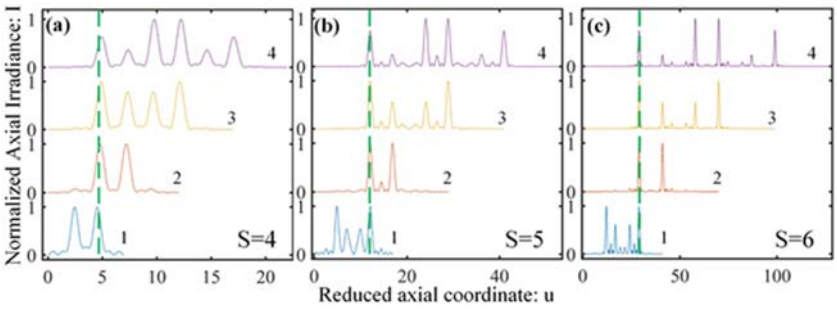

Fig. 8. The axial intensity distributions of the GFiCZPs based on the silver mean sequences of S=(a) 4, (b) 5 and (c) 6, respectively. For the GFiCZPs in each sub-figure, n=0, 1, 2 and 3, respectively.

The corresponding *u* values of two main foci in Fig. 8(b) and Fig. 8(c) are [(4.90, 12.10), (12.09, 16.91), (12.07, 28.93), (24.10, 28.90)] and [(12.11, 28.89), (28.96, 41.04), (28.97, 70.03), (57.95, 70.05)], respectively. Thus, the *u* values of one of two main foci are approximately the same for lines 1-2, 2-3 and 3-4 in Fig. 8(a). The same property applies for the lines in Fig. 8(b) and Fig. 8(c). Therefore, the position of one of two foci can be kept constant for two different GFiCZPs based on the arbitrary-order silver mean sequences.

4. Conclusions

To summarize, we proposed the GFiCZPs to generate a fixed-position focus and more subsidiary foci with varying structural parameters of the zone plates. The corresponding construction method could be applied to other kinds of the bi-focal zone plates. The focusing properties of the GFiCZPs based on the Fibonacci, Thue-Morse, m-bonacci and precious mean sequences were studied in the simulations. The simulation results verified the focusing properties of the GFiCZP, which would have potential applications in the fields of optical trapping, optical imaging and photonic crystal.

Acknowledgements

The research was financially supported by the National Natural Science Foundation of China (NSFC) (Grant Nos. 11674401 and 11747105).

References

[1]. M. Segev, M. Soljačić, J. M. Dudley, Fractal optics and beyond, *Nature Photonics*, Vol. 6, Issue 4, 2012, pp. 209-210.

[2]. W. D. Furlan, G. Saavedra, J. A. Monsoriu, White-light imaging with fractal zone plates, *Optics Letters*, Vol. 32, Issue 15, 2007, pp. 2109-2111.

[3]. S. Tao, X.-C. Yuan, J. Lin, R Burge, Sequence of focused optical vortices generated by a spiral fractal zone plate, *Applied Physics Letters*, Vol. 89, Issue 3, 2006, p. 031105.

[4]. S. Cheng, X. Zhang, W. Ma, S. Tao, Fractal zone plate beam based optical tweezers, *Scientific Reports*, Vol. 6, 2016, p. 34492.

[5]. T. Xia, S. Cheng, S. Tao, The generalized Fibonacci class zone plate, in *Proceedings of the* 1st *International Conference on Optics, Photonics and Lasers (OPAL'18)*, Barcelona, Castelldefels, Spain, 9-11 May 2018, pp. 21-24.

[6]. J. A. Monsoriu, A. Calatayud, L. Remon, W. D. Furlan, G. Saavedra, P. Andres, Bifocal Fibonacci diffractive lenses, *IEEE Photonics Journal*, Vol. 5, Issue 3, 2013, p. 3400106.

[7]. V. Ferrando, F. Giménez, W. D. Furlan, J. A. Monsoriu, Bifractal focusing and imaging properties of Thue–Morse Zone Plates, *Optics Express*, Vol. 23, Issue 15, 2015, pp. 19846-19853.

[8]. W. Ma, S. Tao, S. Cheng, Composite Thue-Morse zone plates, *Optics Express*, Vol. 24, Issue 12, 2016, pp. 12740-12747.

[9]. F. Machado, V. Ferrando, W. D. Furlan, J. A. Monsoriu, Diffractive m-bonacci lenses, *Optics Express*, Vol. 25, Issue 7, 2017, pp. 8267-8273.

[10]. J. A. Monsoriu, M. H. Giménez, W. D. Furlan, J. C. Barreiro, G. Saavedra, Diffraction by m-bonacci gratings, *European Journal of Physics*, Vol. 36, Issue 6, 2015, p. 065005.

[11]. T. Xia, S. Cheng, S. Tao, The generalized mean zone plate, *Laser Physics*, Vol. 28, Issue 6, 2018, p. 066201.

[12]. J. Ke, J. Zhang, Generalized Fibonacci photon sieves, *Applied Optics*, Vol. 54, Issue 24, 2015, pp. 7278-7283.

[13]. T. Xia, S. Cheng, J. Yan, S. Tao, Modified Thue–Morse zone plates with arbitrarily designed high-intensity twin main foci, *Laser Physics*, Vol. 27, Issue 12, 2017, p. 125001.

[14]. E. Macia, Exploiting aperiodic designs in nanophotonic devices, *Reports on Progress in Physics*, Vol. 75, Issue 3, 2012, p. 036502.

[15]. J. A. Monsoriu, C. J. Zapatarodriguez, E. Silvestre, W. D. Furlan, Cantor-like fractal photonic crystal waveguides, *Optics Communications*, Vol. 252, Issue 1-3, 2005, pp. 46-51.

[16]. W. J. Hsueh, C. T. Chen, C. H. Chen, Omnidirectional band gap in Fibonacci photonic crystals with metamaterials using a band-edge formalism, *Physical Review A*, Vol. 78, Issue 1, 2008, p. 013836.

[17]. L. Dal Negro, C. J. Oton, Z. Gaburro, L. Pavesi, P. M. Johnson, A. Lagendijk, R. Righini, M. Colocci, D. S. Wiersma, Light Transport through the Band-Edge States of Fibonacci Quasicrystals, *Physical Review Letters*, Vol. 90, Issue 5, 2003, p. 055501.